Water Science and Engineering 2015, 8(4): 326−334

HOSTED BY

ELSEVIER

CrossMark

Available online at www.sciencedirect.com

Water Science and Engineering

journal homepage: http://www.waterjournal.cn

Seepage and stress analysis of anti-seepage structures constructed with different concrete materials in an RCC gravity dam

Ming-chao Li [a,*], Xin-yu Guo [a], Jonathan Shi [b], Ze-biao Zhu [a]

[a] State Key Laboratory of Hydraulic Engineering Simulation and Safety, Tianjin University, Tianjin 300072, PR China
[b] College of Engineering, Louisiana State University, Baton Rouge, LA 70803, USA

Received 9 December 2014; accepted 8 August 2015
Available online 10 November 2015

Abstract

This study used the finite element method (FEM) to analyze the stress field and seepage field of a roller-compacted concrete (RCC) dam, with an upstream impervious layer constructed with different types of concrete materials, including three-graded RCC, two-graded RCC, conventional vibrated concrete (CVC), and grout-enriched vibrated RCC (GEVR), corresponding to the design schemes S1 through S4. It also evaluated the anti-seepage performance of the imperious layer in the four design schemes under the normal water level and flood-check level. Stress field analysis of a retaining section and discharge section shows that the maximum tensile stress occurs near the dam heel, the maximum compressive stress occurs near the dam toe, and the stress distributions in the four schemes can satisfy the stress control criteria. Seepage field analysis shows that the uplift pressure heads in schemes S3 and S4 descend rapidly in the anti-seepage region, and that the calculated results of daily seepage flow under the steady seepage condition in these two schemes are about 30%−50% lower than those in the other two schemes, demonstrating that CVC and GEVR show better anti-seepage performance. The results provide essential parameters such as the uplift pressure head and seepage flow for physical model tests and anti-seepage structure selection in RCC dams.

Keywords: RCC gravity dam; Concrete partition; Impervious layer; FEM; Seepage field; Stress field

1. Introduction

A roller-compacted concrete (RCC) dam is constructed with the roller-compacted placement method in thin layers of dry lean concrete, composed of mixed sand aggregate and cement (USACE, 1992). Its construction process is much simpler and faster than that of a conventional concrete dam (Yang and Shi, 2010). At present, 450 RCC dams over 30 m are operating in over 30 countries (Hansen, 1997; Nagayama and Jikan, 2003; Jia, 2007). However, some RCC dams have shown serious seepage problems, such as the Willow Creek RCC Gravity Dam, with a height of 56 m, which was built in 1982 in the USA (HWSTI, 1987), and the Xibing RCC Gravity Dam, with a height of 63.5 m, which was built in 1985 in China (Ye et al., 2005).

Although the permeability of RCC is very low and comparable to conventional concrete, the seepage features of an RCC dam is different from those of a conventional concrete dam (Banthia et al., 1992; Chai et al., 2005). Rolling and compacting dry lean concrete layer by layer causes the permeability of construction interfaces and joints to be relatively high, and seepage channels may even form in the dam body. In order to overcome this problem, an upstream impervious structure must be properly designed and constructed (Hong et al., 2014). A variety of impervious structures have been used in RCC dams around the world. For example, some RCC dams were constructed with waterproof

This work was supported by the National Basic Research Program of China (Grant No. 2013CB035903) and the National Natural Science Foundation of China (Grants No. 51321065 and 51209159).
* Corresponding author.
E-mail address: lmc@tju.edu.cn (Ming-chao Li).
Peer review under responsibility of Hohai University.

http://dx.doi.org/10.1016/j.wse.2015.10.001

membranes in the USA (Hansen, 1997). In Japan, a layer of conventional vibrated concrete (CVC), used as an impervious layer, with a thickness of 2−3 m, has typically been poured on the upstream face of an RCC dam (Nagayama and Jikan, 2003). Polyvinyl chloride films were used in the Trigomil Dam in Mexico and in the Copperfield Dam in Australia (Jansen, 1989). Grout-enriched vibrated RCC (GEVR) has been widely used in anti-seepage structures in RCC dams in China (Sun et al., 2004).

Based on design functions, such as seepage control, crack resistance, and frost resistance, a gravity dam body can be partitioned into different parts (Zhou and Dang, 2011), as shown in Fig. 1.

The finite element method (FEM) is currently used to simulate complex geometrical shapes and boundary conditions, and two-dimensional (2D) or three-dimensional (3D) models are used to analyze the thermal stress and cracks in concrete dams. Luna and Wu (2000) developed a 3D finite element program to simulate the temperature and stress changes in the construction process of an RCC gravity dam. Chen et al. (2003) conducted a 3D thermal stress analysis of a high RCC dam and predicted the internal temperature distribution of the dam body. Bayagoob et al. (2010) performed a thermal stress analysis of an RCC arch dam by taking into account the construction sequence, environmental temperature change, and wind speed. Gaspar et al. (2014) modeled the temperature field of an RCC gravity dam based on FEM simulation. Some studies have been performed focusing on cracking analysis. Cervera et al. (2000) assessed the risk of tensile cracking through numerical simulation of the construction process of an RCC dam. Li et al. (2010) used a nonlinear FEM to obtain the crack length of the foundation surface of a gravity dam. Cao et al. (2012) simulated thermal cracks in a concrete overflow dam using the 3D FEM. Zhang et al. (2013) conducted a seismic cracking analysis of a concrete gravity dam based on an extended FEM. However, research on numerical analysis of the impervious layer in an RCC dam is limited. Chai et al. (2005) proposed a mathematical model for analysis of coupled seepage and stress fields in RCC dams. Xie and Chen (2005) used a 3D finite element relocating mesh method to simulate the temperature field of impervious layers of different thicknesses, constructed with different materials, in an RCC dam.

In practice, there are some limitations in the design scheme of an upstream impervious layer determined by model experiments or analogies. The numerical simulation analysis method can help contrast and evaluate design schemes. The purpose of this research is to compute and evaluate the stress and seepage fields of different anti-seepage designs in an RCC dam. It covers the following issues: (1) analysis of concrete materials used in four different anti-seepage design schemes, (2) stress field analysis of the four schemes, and (3) evaluation of the anti-seepage effect of the four schemes.

2. Anti-seepage design schemes of RCC dam

The Huangdeng RCC Gravity Dam, currently under construction and located on the Lancang River in Southwest China, was selected as a case study. Its maximum height is 203 m, and the crest length is 464 m. The dam body is divided into 20 sections, as shown in Fig. 2, of which sections 1 through 7 and sections 12 through 15 are the retaining sections; sections 8 and 11 are designed for flood discharge, with an outlet at the bottom in each section; sections 9 and 10 are also discharge sections; and sections 16 through 20 are the water intake sections.

Four anti-seepage design schemes were studied for the project, as shown in Table 1. The concrete materials used in parts I, IV, V, and VI, were the same for each of the schemes, with the main difference lying in the concrete materials used in parts II and III. There was no special design for the impervious layer in scheme S1, and three-graded RCC were used in parts II and III. The impervious layer was specially designed in schemes S2, S3, and S4, in which two-graded

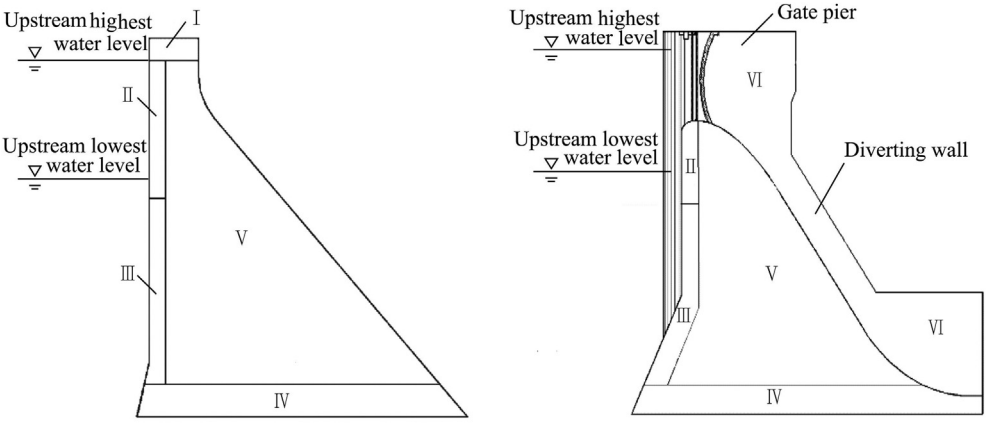

Fig. 1. Typical parts in RCC gravity dam body.

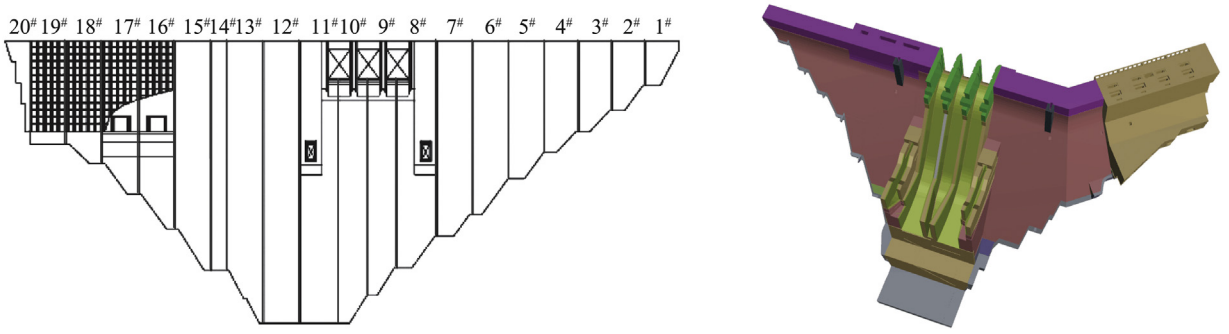

(a) Elevation view from upstream

(b) Three-dimensional visualization from downstream

Fig. 2. Huangdeng RCC Gravity Dam.

Table 1
Four anti-seepage design schemes using different concrete materials

Scheme	Material for different parts					
	I	II	III	IV	V	VI
S1	Three-graded CVC (C_{90}20W8F100)	Three-graded RCC (RCC_{90}20W6F100)	Three-graded RCC (RCC_{90}25W8F100)	Three-graded CVC (C_{90}25W12F100)	Three-graded RCC (RCC_{90}20W6F100)	Two-graded CVC (C_{28}50W8F150)
S2		Two-graded RCC (RCC_{90}20W10F150)	Two-graded RCC (RCC_{90}25W12F150)			
S3		Three-graded CVC (C_{90}25W10F200)	Two-graded CVC (C_{28}25W8F100)			
S4		Two-graded GEVR (C_{90}25W12F150)	Two-graded GEVR (C_{90}25W12F150)			

Table 2
Parameters of different concrete materials

Material	Elasticity modulus (10^{10} Pa)	Poisson ratio	Permeability coefficient in normal direction (cm/s)	Permeability coefficient in tangential direction (cm/s)	Permeability coefficient of dam body (cm/s)
C_{90}20W8F100	2.55	0.167	1.00×10^{-10}	1.00×10^{-10}	1.00×10^{-10}
C_{90}25W10F200	2.80	0.167	1.00×10^{-10}	1.00×10^{-10}	1.00×10^{-10}
C_{90}25W12F100	2.80	0.167	1.00×10^{-10}	1.00×10^{-10}	1.00×10^{-10}
C_{28}50W8F150	3.40	0.167	1.00×10^{-10}	1.00×10^{-10}	1.00×10^{-10}
C_{28}25W8F100	2.30	0.200	1.00×10^{-10}	1.00×10^{-10}	1.00×10^{-10}
RCC_{90}25W8F100	3.10	0.200	1.00×10^{-9}	1.78×10^{-7}	1.00×10^{-9}
RCC_{90}20W6F100	2.70	0.200	1.00×10^{-9}	1.78×10^{-7}	1.00×10^{-9}
RCC_{90}25W12F150	2.80	0.200	1.00×10^{-9}	2.25×10^{-8}	1.00×10^{-9}
RCC_{90}20W10F150	2.50	0.200	1.00×10^{-9}	2.25×10^{-8}	1.00×10^{-9}
C_{90}25W12F150*	2.80	0.200	1.00×10^{-9}	1.00×10^{-9}	1.00×10^{-9}
Foundation rock	2.20	0.250	1.00×10^{-6}	1.00×10^{-6}	1.00×10^{-6}

Note: * means two-graded GEVR.

RCC, CVC, and GEVR were used, respectively. The parameters of different materials are listed in Table 2.

In order to evaluate the anti-seepage performance of the impervious layer in these design schemes, a typical retaining section (section 5) with a maximum height of 110 m and a discharge section (section 8) with a maximum height of 200 m were selected for stress and seepage analyses with FEM.

3. Finite element simulation method

3.1. Simulation of dam stress field

A gravity dam maintains its stability relying on its body weight, with a balance reached between the compressive stress induced by its weight and the tensile stress induced by the water pressure at the heel. It is important that the tensile stress meets the following requirements: (1) the distribution area of the first principal tensile stress σ_1 in the foundation does not exceed the center line of the curtain; or (2) the total length of the tensile stress zone at the dam heel and toe does not exceed 10% of the bottom width of the dam (Zhou and Dang, 2011; Zhou and Chang, 2002).

FEM is used under three basic assumptions (Rombach, 2011): (1) cracking may occur in the x, y, and z directions; (2) if cracking occurs, the smeared crack model, a plastic concrete model, will be used; and (3) concrete is initially isotropic.

The stress constitutive equation is constructed as a multi-linear kinematic hardening plasticity model:

$$\sigma_c = \begin{cases} f_c\left[1-\left(1-\dfrac{\varepsilon_c}{\varepsilon_0}\right)^2\right] & \varepsilon_c \le \varepsilon_0 \\ f_c\left[1-0.15\left(\dfrac{\varepsilon_c-\varepsilon_0}{\varepsilon_{cu}-\varepsilon_0}\right)\right] & \varepsilon_0 < \varepsilon_c \le \varepsilon_{cu} \end{cases} \quad (1)$$

where σ_c and ε_c are the compressive stress and strain of an element, respectively; f_c is the peak pressure; and ε_0 and ε_{cu} are the peak strain and ultimate compressive strain, respectively.

The displacement equation of an element is obtained through the generalized Hooke law and the virtual work principle as follows:

$$\boldsymbol{u}_e = \boldsymbol{N}\boldsymbol{\delta} \quad (2)$$

where $\boldsymbol{u}_e$ is the elementary displacement vector, $\boldsymbol{N}$ is the shape function matrix, and $\boldsymbol{\delta}$ is the nodal displacement matrix.

Any node of an element is subject to two forces: the internal load induced by element deformation and the external load. They are balanced if the composite force is zero. Therefore, the total equilibrium equation can be formulated as follows:

$$\boldsymbol{K}\boldsymbol{\delta} = \boldsymbol{P} \quad (3)$$

where $\boldsymbol{K}$ is the global stiffness matrix, and $\boldsymbol{P}$ is the global nodal force matrix.

Eq. (3) can be solved with the matrix inversion method, and the nodal displacement matrix is $\boldsymbol{K}^{-1}\boldsymbol{P}$. The strain and stress at each element can be obtained by

$$\boldsymbol{\varepsilon} = \boldsymbol{B}\boldsymbol{\delta} \quad \boldsymbol{\sigma} = \boldsymbol{D}\boldsymbol{\varepsilon} \quad \boldsymbol{F} = \boldsymbol{k}\boldsymbol{\delta} \quad (4)$$

where $\boldsymbol{B}$ is the elementary strain matrix, $\boldsymbol{D}$ is the elementary elasticity modulus matrix, $\boldsymbol{F}$ is the elementary force matrix, $\boldsymbol{k}$ is the elementary stiffness matrix, and $\boldsymbol{\sigma}$ and $\boldsymbol{\varepsilon}$ are the elementary stress and strain vectors, respectively.

3.2. Simulation of dam seepage field

Seepage flow can be simulated using ANSYS (ANSYS Inc., 2009). The goal is to determine the free surface of a seepage field and a seepage channel by solving the water head function. Seepage analysis of RCC materials is based on Darcy's law (Freeze, 1994):

$$v = \frac{Q_S}{A} = -k_s\frac{dh}{dl} = k_s J \quad (5)$$

where v is the average velocity, Q_S is the seepage flow, A is the cross-sectional area, k_s is the permeability coefficient, h is the piezometric head, l is the seepage path length, and J is the seepage gradient.

The differential equation of a steady seepage field is

$$\frac{\partial}{\partial x}\left(k_{sx}\frac{\partial h}{\partial x}\right) + \frac{\partial}{\partial y}\left(k_{sy}\frac{\partial h}{\partial y}\right) + \frac{\partial}{\partial z}\left(k_{sz}\frac{\partial h}{\partial z}\right) = 0 \quad (6)$$

where k_{sx}, k_{sy}, and k_{sz} are the permeability coefficients in the x, y, and z directions.

The boundary conditions are as follows:

$$\begin{cases} h|_{\Gamma_1} = f_1(x,y,z) \\ k_{sn}\dfrac{\partial h}{\partial n}\Big|_{\Gamma_2} = f_2(x,y,z) \end{cases} \quad (7)$$

where Γ_1 and Γ_2 are the initially known boundaries for water head and flow analysis, respectively; $f_1(x,y,z)$ is the initial water head boundary condition at boundary Γ_1; k_{sn} is the permeability coefficient in the normal direction of boundary Γ_2; and $f_2(x,y,z)$ is the initial flow boundary condition at boundary Γ_2.

The computation is performed using the birth-death element technology and the self-adaptive mesh technique in ANSYS. The water head of a free surface is equal to the atmospheric pressure. Thus, the elements below the free surface are killed, and the elements above the free surface are activated. The birth or death features of elements are adjusted and recalculated until the expected accuracy is satisfied.

4. Results and discussion

4.1. Finite element model under loading condition

The 3D finite element model of the dam is shown in Fig. 3. The meshes of the dam foundation were generated through uniform mapping. The meshes were divided using the sweeping method in the regular parts of the dam body, and free meshing was used in the irregular dam parts, including the non-overflow dam section with high varying rates of curvature. In addition, sparse meshes were used in the parts with low stress, such as the upper part of the dam and the part near the dam foundation, in order to reduce the computation time. However, at the bottom of the dam, especially at the toe and heel, the compressive and tensile stresses were high. Thus, the meshes there were refined to improve the accuracy.

The main loads of the dam under two different conditions are as follows: for the condition at the normal water level, the loads include the gravity, hydrostatic pressure, uplift pressure, silt pressure, wave pressure, and temperature load; for the condition at the flood-check level, hydrodynamic pressure

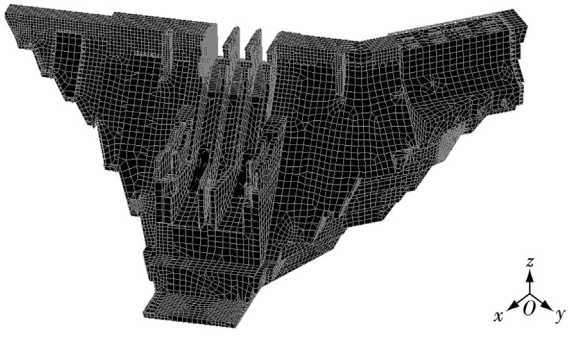

Fig. 3. Three-dimensional mesh model.

occurs in addition to the loads described above. The meshes of sections 5 and 8 are shown in Fig. 4, where different colors refer to different materials, and lines with arrows show the direction and distribution of the hydrostatic pressure and uplift pressure. The hydrostatic pressure and uplift pressure are linearly distributed along the edge of the dam, as indicated in Fig. 4. The degrees of freedom at the bottom are determined by the normal constraint condition. The mechanical parameters of the concrete materials are obtained from field tests and analyses (Gu et al., 2010).

4.2. Stress field analysis

Figs. 5 and 6 show the stress distributions in sections 5 and 8 under the normal water level and flood-check level in scheme S4, where σ_1 and σ_3 are the first and third principal stresses, respectively. It can be found that the maximum tensile stress occurs near the dam heel, as shown in Figs. 5(a) and (b), and the maximum compressive stress occurs near the dam toe, as shown in Figs. 5(c) and (d). The stress results of retaining section 5 and discharge section 8 in the four

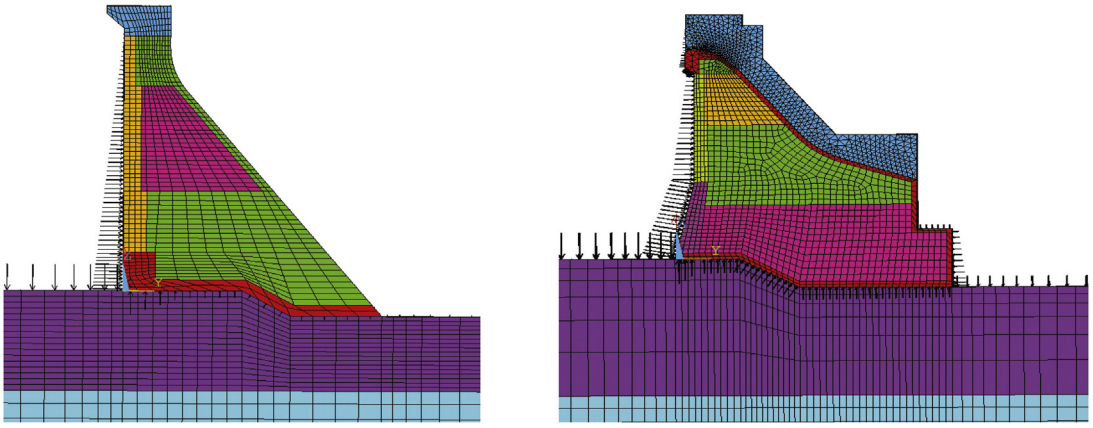

(a) Retaining section 5 (b) Discharge section 8

Fig. 4. Finite element models of retaining section 5 and discharge section 8 under loading condition.

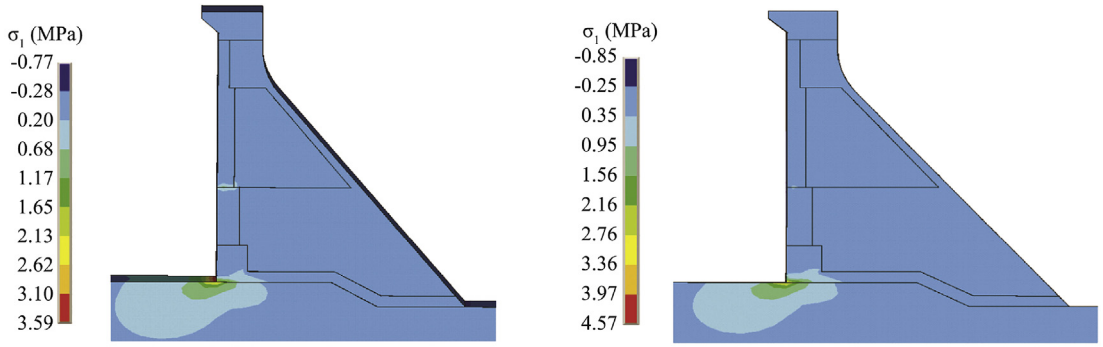

(a) First principal stress distribution under normal water level (b) First principal stress distribution under flood-check level

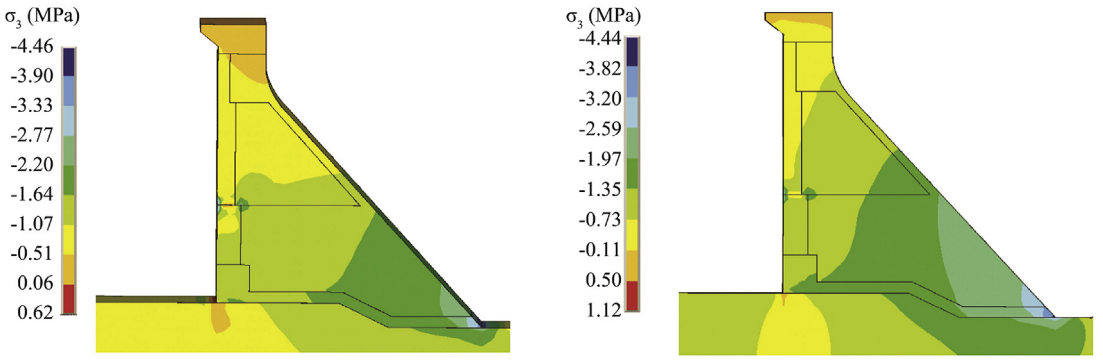

(c) Third principal stress distribution under normal water level (d) Third principal stress distribution under flood-check level

Fig. 5. Stress distributions in retaining section 5 under different water levels in scheme S4.

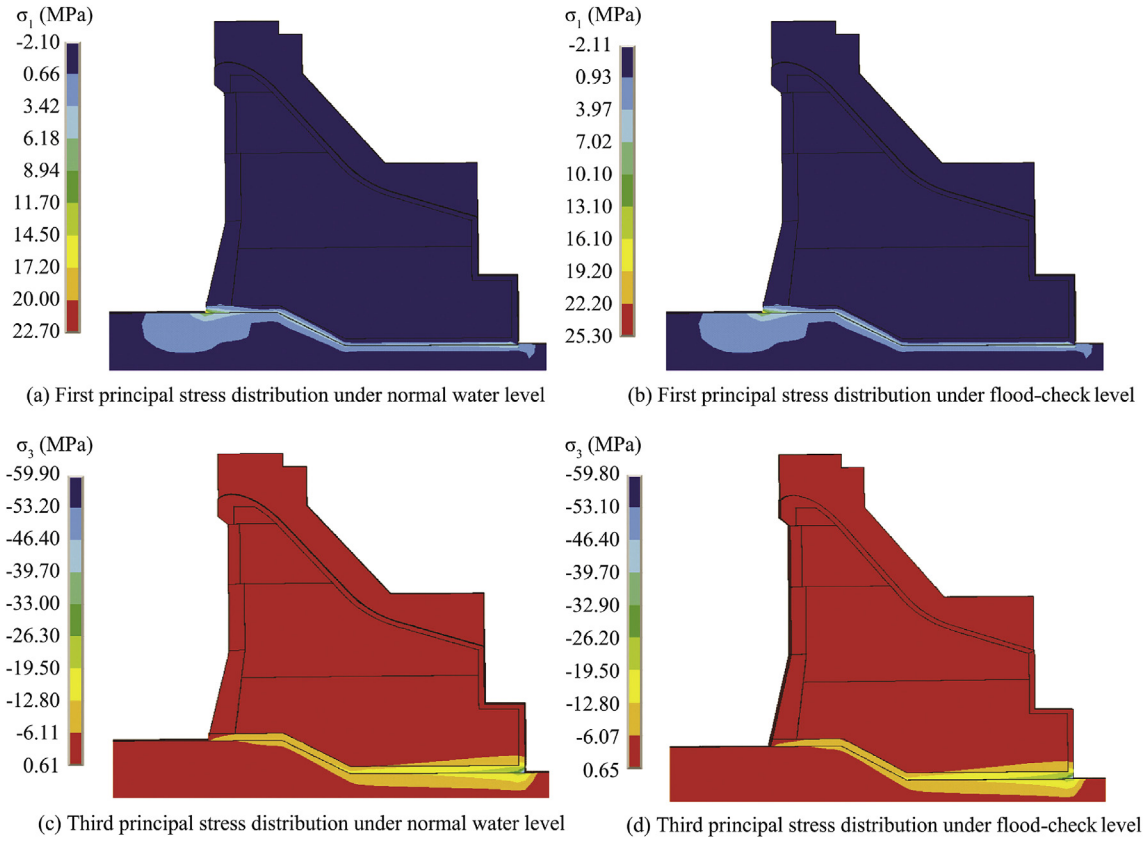

(a) First principal stress distribution under normal water level

(b) First principal stress distribution under flood-check level

(c) Third principal stress distribution under normal water level

(d) Third principal stress distribution under flood-check level

Fig. 6. Stress distributions in discharge section 8 under different water levels in scheme S4.

schemes under the normal water level and flood-check level are listed in Tables 3 and 4, respectively, where σ_{1tp} and σ_{3tp} are the maximum values of the first and third principal tensile stresses, respectively, σ_{1cp} and σ_{3cp} are maximum values of the first and third principal compressive stresses, respectively, and the width ratio is the ratio of the total length of the tensile stress zone to the bottom width of the dam. From Tables 3 and 4, we can see that the maximum values in different

Table 3
Stress results of retaining section 5 in different schemes.

Water level	Scheme	σ_{1tp} (MPa)	σ_{3tp} (MPa)	Tensile stress zone width (m)	Width ratio (%)	σ_{1cp} (MPa)	σ_{3cp} (MPa)
Normal water level	S1	3.60	0.63	5.57	6.2	−0.76	−4.40
	S2	3.60	0.64	5.35	6.0	−0.76	−4.43
	S3	3.60	0.66	5.57	6.2	−0.76	−4.42
	S4	3.59	0.62	5.98	6.7	−0.77	−4.46
Flood-check level	S1	4.59	1.14	5.88	6.6	−0.84	−4.43
	S2	4.59	1.15	5.39	6.0	−0.84	−4.43
	S3	4.60	1.16	5.88	6.6	−0.84	−4.43
	S4	4.57	1.12	6.03	6.8	−0.85	−4.44

Table 4
Stress results of discharge section 8 in different schemes.

Water level	Scheme	σ_{1tp} (MPa)	σ_{3tp} (MPa)	Tensile stress zone width (m)	Width ratio (%)	σ_{1cp} (MPa)	σ_{3cp} (MPa)
Normal water level	S1	21.50	0.60	11.58	7.2	−2.06	−58.40
	S2	22.30	0.67	11.07	6.9	−2.09	−59.90
	S3	22.00	0.60	10.50	6.5	−2.06	−58.30
	S4	22.70	0.61	12.35	7.7	−2.10	−59.90
Flood-check level	S1	24.90	0.65	11.30	7.0	−2.12	−59.90
	S2	25.70	0.72	10.87	6.7	−2.14	−61.40
	S3	26.20	0.66	12.58	7.8	−2.15	−61.40
	S4	25.30	0.65	9.87	6.1	−2.11	−59.80

schemes are almost the same for the same water level, and these maximum values spread across a reasonable range according to engineering practice. Compared with the results under the normal water level, the stress distributions under the flood-check level are similar but with higher values, as expected due to higher loads induced by higher water levels. The width ratios in Tables 3 and 4 show that the stress distributions in the four schemes can meet the stress control criteria given in Section 3.1. The stress results provide a basis for seepage analysis.

4.3. Seepage field analysis

Since the results under the normal water level and flood-check level are similar, the following analysis focuses on the results under the normal water level. The water head distributions in retaining section 5 and discharge section 8 under the steady seepage condition are shown in Figs. 7 and 8, respectively. The uplift pressure head variations in two typical cutting planes in the four schemes are compared, as shown in Fig. 9, where the horizontal axis means the distance from the upstream side along the transverse direction of the dam foundation.

Without a special design of the impervious layer in scheme S1, the attenuation of water head along the transverse direction of the dam foundation is slow and linear, as shown in Figs. 7(a) and 9. With seepage flow penetrating in the direction perpendicular to the equipotential line, water permeates the dam body, which may cause hydraulic fractures. Figs. 7 and 8 show that the water head distributions in schemes S3 and S4 are almost the same, and the water head descends rapidly in the impervious layer in schemes S2 through S4. Compared with the impervious layer in scheme S1, the specially designed impervious layers in schemes S2 through S4 can experience higher water pressure, while the dam body suffers lower water head. In addition, the water head contour trend from S1 to S4 indicates that the direction of seepage flow will change from the direction parallel to the dam foundation to that perpendicular to the dam foundation, which is beneficial to dam safety. Considering that potential seepage channels occur when two-graded RCC is used in the impervious layer, CVC or GEVR is more suitable for upstream anti-seepage structures.

The computed daily seepage flows through retaining section 5 and discharge section 8 in the four schemes under the normal water level are listed in Table 5. The rate of seepage flow in scheme S1 is greater than those in the other three schemes, and the values in schemes S3 and S4 are very close and even lower than that in section S2, indicating that schemes S3 and S4 are more suitable for the upstream anti-seepage structure.

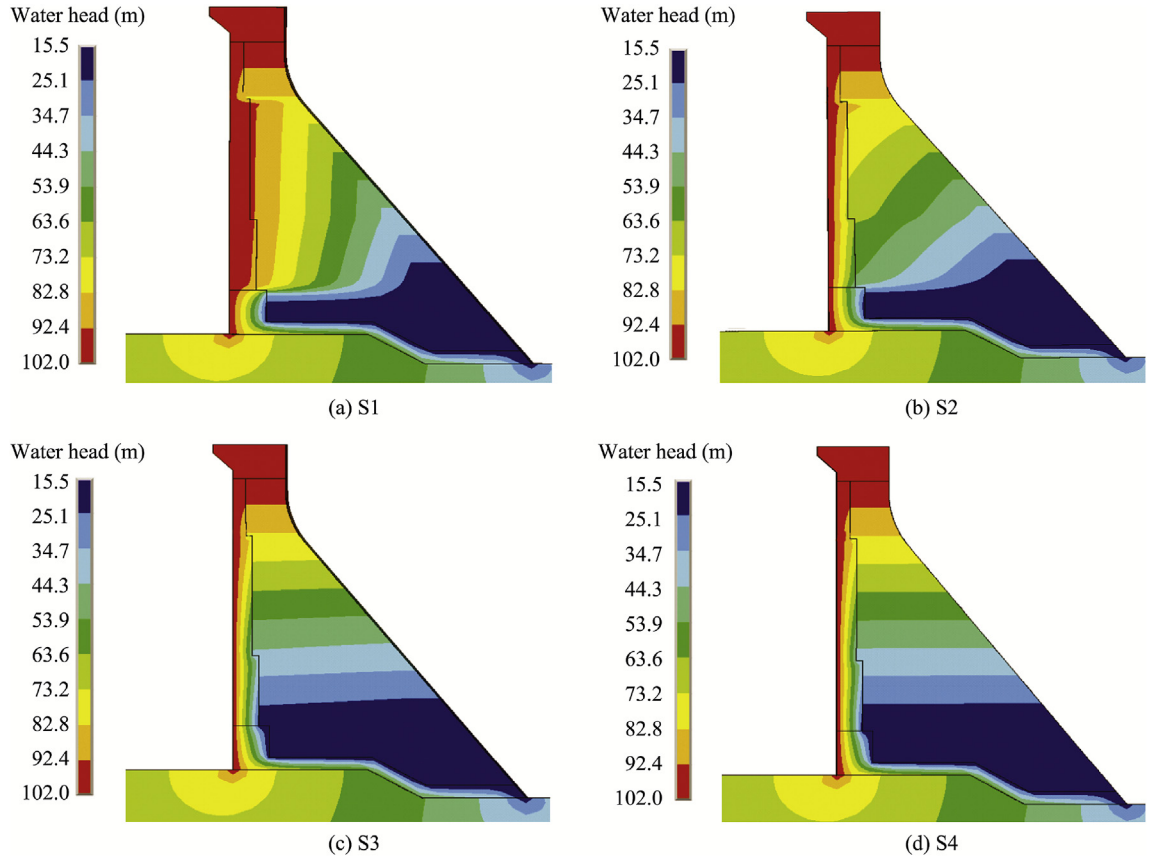

Fig. 7. Water head distributions in retaining section 5 under normal water level in different schemes.

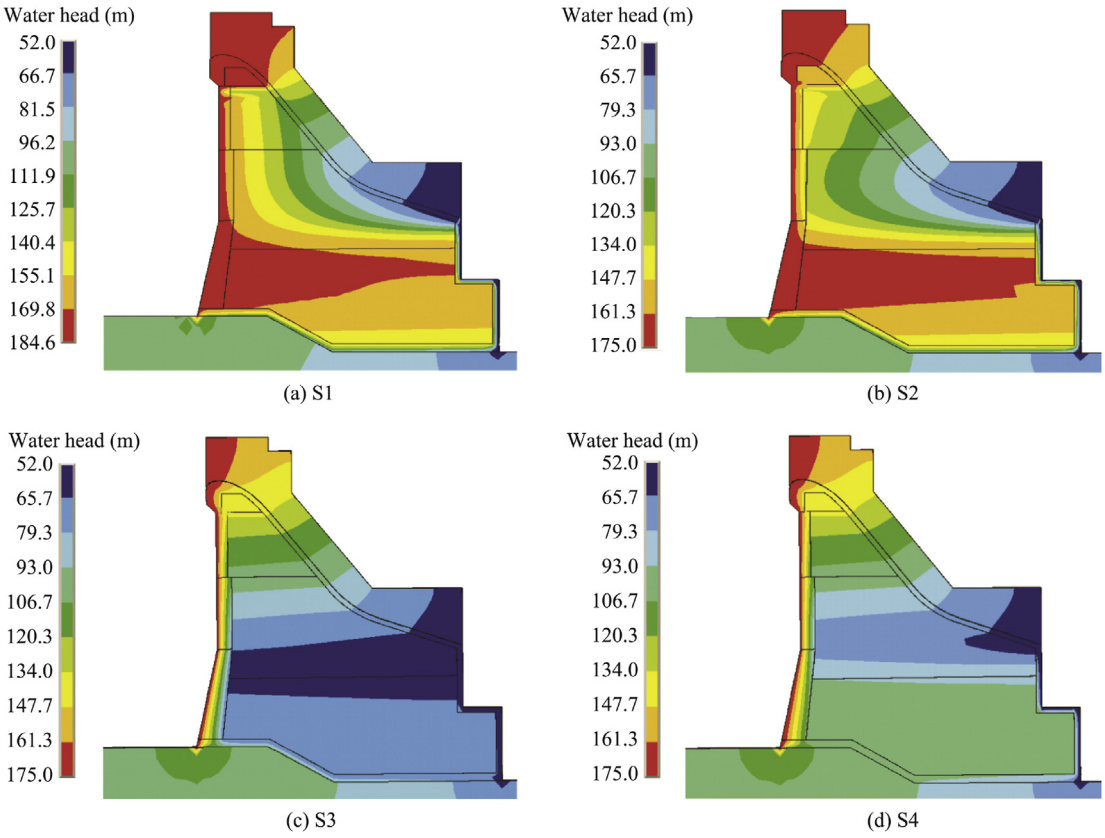

Fig. 8. Water head distributions in discharge section 8 under normal water level in different schemes.

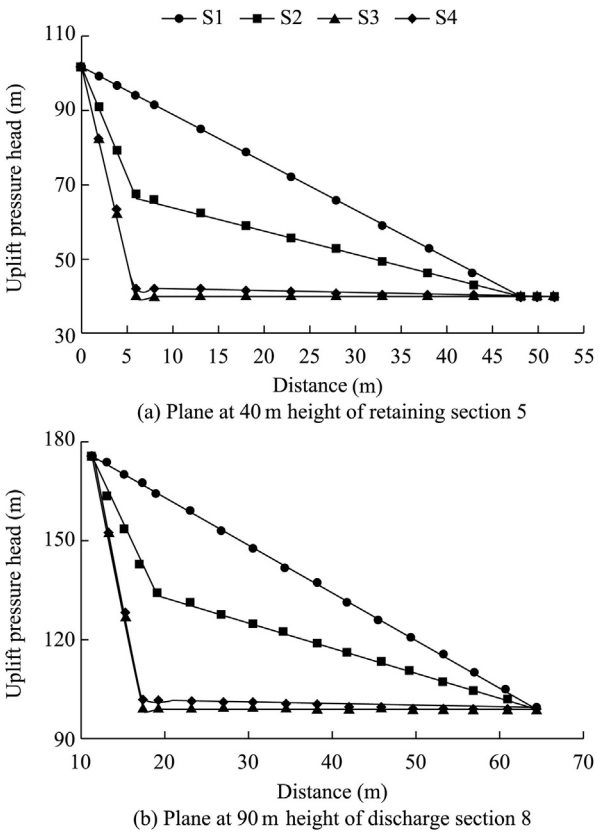

Fig. 9. Comparison of uplift pressure head curves in four schemes for retaining section 5 and discharge section 8.

Table 5
Comparison of seepage flows through retaining section 5 and discharge section 8 under normal water level in four schemes.

Scheme	Rate of seepage flow (m^3/d)	
	Retaining section 5	Discharge section 8
S1	1.10	0.69
S2	0.73	0.51
S3	0.55	0.34
S4	0.56	0.35

5. Conclusions

Based on the concrete partitioning of a gravity dam, four schemes for the impervious layer in an RCC dam were designed using different concrete materials, which are three-graded RCC and two-graded RCC, CVC, and GEVR, respectively.

Three-dimensional FEM was used to compute the stress and seepage fields of two typical dam sections under complex conditions, including one retaining section and one discharge section. The results of the stress field analysis under the normal water level and flood-check level show that the maximum tensile stress occurs near the dam heel, the maximum compressive stress occurs near the dam toe, and the stress distributions in the four design schemes can meet the stress control criteria of an RCC dam. However, according to the results of the water head distributions and seepage flows under the steady seepage condition, the impervious

layer built with three-graded RCC shows a poor seepage control effect. The two-graded RCC layer can improve the anti-seepage performance but seepage channels may develop. The CVC and GEVR impervious layers show a better performance with rapidly descending water heads in the anti-seepage region and lower rates of seepage flow. They are suitable for the upstream anti-seepage structure in an RCC dam. The results can provide useful information for selecting anti-seepage structures in RCC dams and for calibrating results from physical models.

References

ANSYS Inc., 2009. ANSYS User's Guide, Release 12.1. ANSYS Inc., Canonsburg.

Banthia, N., Pigeon, M., Marchand, J., Boisvert, J., 1992. Permeability of roller compacted concrete. J. Mater. Civ. Eng. 4(1), 27−40. http://dx.doi.org/10.1061/(ASCE)0899-1561(1992)4:1(27).

Bayagoob, K.H., Noorzaei, J., Abdulrazeg, A.A., Al-Karni, A.A., Jaafar, M.S., 2010. Coupled thermal and structural analysis of roller compacted concrete arch dam by three-dimensional finite element method. Struct. Eng. Mech. 36(4), 401−419. http://dx.doi.org/10.12989/sem.2010.36.4.401.

Cao, F.J., Fang, G.H., Ma, X.G., Hu, Z.N., 2012. Simulation analysis of crack cause of concrete overflow dam for Hadashan Hydro Project by 3-D FEM. Syst. Eng. Procedia 2(3), 48−54. http://dx.doi.org/10.1016/j.sepro.2011.11.007.

Cervera, M., Oliver, J., Prato, T., 2000. Simulation of construction of RCC dams, II: stress and damage. J. Struct. Eng. 126(9), 1062−1069. http://dx.doi.org/10.1061/(ASCE)0733-9445(2000)126:9(1062).

Chai, J.R., Li, K.H., Wu, Y.Q., Li, S.Y., 2005. Coupled seepage and stress fields in roller compacted concrete dam. Commun. Numer. Methods Eng. 21(1), 13−21. http://dx.doi.org/10.1002/cn m.722.

Chen, Y.L., Wang, C.J., Li, S.Y., Chen, L.J., 2003. The effect of construction designs on temperature field of a roller compacted concrete dam: A simulation analysis by a finite element method. Can. J. Civ. Eng. 30(6), 1153−1156. http://dx.doi.org/10.1139/l03-076.

Freeze, R.A., 1994. Henry Darcy and the fountains of Dijon. Ground Water 32(1), 23−30. http://dx.doi.org/10.1111/j.1745-6584.1994.tb00606.x.

Gaspar, A., Lopez-Caballero, F., Modaressi-Farahmand-Razavi, A., Gomes-Correia, A., 2014. Methodology for a probabilistic analysis of an RCC gravity dam construction: Modelling of temperature, hydration degree and ageing degree fields. Eng. Struct. 65, 99−110. http://dx.doi.org/10.1016/j.engstruct.2014.02. 002.

Gu, C.S., Li, B., Xu, G.L., Yu, H., 2010. Back analysis of mechanical parameters of roller compacted concrete dam. Sci. China Technol. Sci. 53(3), 848−853. http://dx.doi.org/10.1007/s11431-010-0053-0.

Hansen, K.D., 1997. Current RCC dam activity in the USA. Hydropower Dams 4(5), 62−65.

Hong, Y.W., Du, C.B., Jiang, S.Y., 2014. Design Theory and Practice of High RCC Gravity Dam under Complex Conditions. Science Press, Beijing (in Chinese).

HWS Technologies Inc. (HWSTI), 1987. Annual Safety Inspection Report for Willow Creek Dam. HWS Technologies Inc., Lincoln.

Jansen, R.B., 1989. Advanced Dam Engineering for Design, Construction, and Rehabilitation. Springer, US, New York.

Jia, J.S., 2007. New Progress on Roller Compacted Concrete Dams. China Water and Power Press, Beijing (in Chinese).

Li, T.C., Li, D.D., Wang, Z.Q., 2010. Tensile reliability analysis for gravity dam foundation surface based on FEM and response surface method. Water Sci. Eng. 3(2), 233−240. http://dx.doi.org/10.3882/j.issn.1674-2370.2010.02.011.

Luna, R., Wu, Y., 2000. Simulation of temperature and stress fields during RCC dam construction. J. Constr. Eng. Manag. 126(5), 381−388. http://dx.doi.org/10.1061/(ASCE)0733-9364(2000)126:5(381).

Nagayama, I., Jikan, S., 2003. 30 years' history of roller-compacted concrete dams in Japan. In: Proceedings of 4th International Symposium on Roller Compacted Concrete. Madrid, pp. 27−38.

Rombach, G.A., 2011. Finite-element Design of Concrete Structures, second ed. ICE Publishing, London.

Sun, G.Y., Wang, S.Y., Feng, S.R., 2004. High Roller Compacted Concrete Dams. China Electric Power Press, Beijing (in Chinese).

U.S. Army Corps of Engineers (USACE), 1992. Roller-compacted Concrete, Engineering Manual, No. 1110-2-2006. U.S. Army Corps of Engineers, Washington, D.C.

Xie, H.W., Chen, Y.L., 2005. Determination of the type and thickness for impervious layer in RCC dam. Adv. Eng. Softw. 36(8), 561−566. http://dx.doi.org/10.1016/j.advengsoft.2005.01.001.

Yang, L., Shi, J.J., 2010. Experimental study on the impact of rainfall on RCC construction. J. Constr. Eng. Manag. 136(5), 477−483. http://dx.doi.org/10.1061/(ASCE)CO.1943-7862.0000156.

Ye, Y.X., Liu, G.T., Li, P.H., Chen, F.Q., 2005. Dealing with leakage of Xibing roller compacted concrete thin arch dam. Adv. Sci. Technol. Water Resour. 25(3), 27−31. http://dx.doi.org/10.3880/j.issn.1006-7647.2005.03.009 (in Chinese).

Zhang, S.R., Wang, G.H., Yu, X.R., 2013. Seismic cracking analysis of concrete gravity dams with initial cracks using the extended finite element method. Eng. Struct. 56, 528−543. http://dx.doi.org/10.1016/j.engstruct.2013.05.037.

Zhou, J.P., Dang, L.C., 2011. Handbook of Hydraulic Structure Design: Concrete Dams, second ed. China Water and Power Press, Beijing (in Chinese).

Zhou, W., Chang, X.L., 2002. Research on optimization of the whole configuration of RCC gravity dam based on FEM. J. Hydroelectr. Eng. 76, 3−9. http://dx.doi.org/10.3969/j.issn.100-1243.2002.01.002 (in Chinese).